

# Antiproton-nucleus electromagnetic annihilation as a way to access the proton timelike form factors

H. Fonvieille<sup>1</sup> and V.A. Karmanov<sup>2</sup>

<sup>1</sup> Laboratoire de Physique Corpusculaire, Université Blaise Pascal, IN2P3, 63177 Aubières Cedex, France

<sup>2</sup> Lebedev Physical Institute, Leninsky Prospekt 53, 119991 Moscow, Russia

Received: ... / Revised version: ...

**Abstract** Contrary to the reaction  $\bar{p}p \rightarrow e^+e^-$  with a high momentum incident antiproton on a free target proton at rest, in which the invariant mass  $\mathcal{M}$  of the  $e^+e^-$  pair is necessarily much larger than the  $\bar{p}p$  mass  $2m$ , in the reaction  $\bar{p}d \rightarrow e^+e^-n$  the value of  $\mathcal{M}$  can take values near or below the  $\bar{p}p$  mass. In the antiproton-deuteron electromagnetic annihilation, this allows to access the proton electromagnetic form factors in the time-like region of  $q^2$  near the  $\bar{p}p$  threshold. We estimate the cross section  $d\sigma_{\bar{p}d \rightarrow e^+e^-n}/d\mathcal{M}$  for an antiproton beam momentum of 1.5 GeV/c. We find that near the  $\bar{p}p$  threshold this cross section is about 1 pb/MeV. The case of heavy nuclei target is also discussed. Elements of experimental feasibility are presented for the process  $\bar{p}d \rightarrow e^+e^-n$  in the context of the PANDA project.

**PACS.** 25.43.+t Antiproton-induced reactions – 14.20.Dh Properties of protons and neutrons – 13.40.Gp Electromagnetic form factors

## 1 Introduction

A lot of efforts are devoted to understanding the structure of the nucleon, the building block of matter. The underlying theory is the field theory of strong interaction, QCD, in its non-perturbative regime. Electromagnetic properties of the nucleon are fundamental pieces to this puzzle. Among them, the electromagnetic form factors of the proton and the neutron are basic observables, which are the goal of extensive measurements. In the spacelike region, i.e. for a virtual photon four-momentum squared  $q^2 < 0$ , these form factors give information about the spatial distribution of electric charge and magnetization inside the nucleon. In the timelike region ( $q^2 > 0$ ) they tell us about the dynamics of the nucleon-antinucleon ( $N\bar{N}$ ) interaction.

A fully consistent description of the nucleon form factors should include both domains, of spacelike and timelike  $q^2$ , since these domains are related by crossing symmetry. Such theoretical models are generally based on dispersion relations [1,2,3] or semi-phenomenological approaches [4,5]. They predict a smooth behavior of the form factor in the measured regions, but a peaked behavior in the timelike region below the  $N\bar{N}$  threshold ( $0 < q^2 < 4m^2$ , where  $m$  is the nucleon mass), due to

poles in the amplitude (see e.g. fig. 1, taken from [6]). These poles are phenomenological inputs, built from meson exchange, and their properties are fitted to the data in the measured regions. The corresponding irregularities in form factors are related to the transition of  $p\bar{p}$  to vector mesons which can decay in  $e^+e^-$  pair via a virtual photon.

The mesons with a mass near the  $p\bar{p}$  mass can have a quasinuclear nature, i.e., they can be formed by bound states and resonances in the  $p\bar{p}$  system. Such vector mesons were predicted in the papers [7,8]. Note that such mesons can be formed not only in the  $p\bar{p}$  system but in  $N\bar{N}$  in general and they can have not only vector quantum numbers. A review on quasinuclear mesons in the  $N\bar{N}$  system is given in [9].

The under-threshold region ( $0 < q^2 < 4m^2$ ) is called unphysical because it cannot be accessed experimentally by an on-shell process. Some experiments have been performed in the vicinity of the  $N\bar{N}$  threshold, either in  $p\bar{p} \rightarrow e^+e^-$  at LEAR [10] or in the inverse channel  $e^+e^- \rightarrow p\bar{p}$  at Babar [11], but they cannot go below this physical threshold. However, a nucleus provides nucleons with various momenta, in modulus and direction, and also various degrees of off-shellness. Therefore it offers the possibility to produce an  $N\bar{N}$  electromagnetic annihilation with an

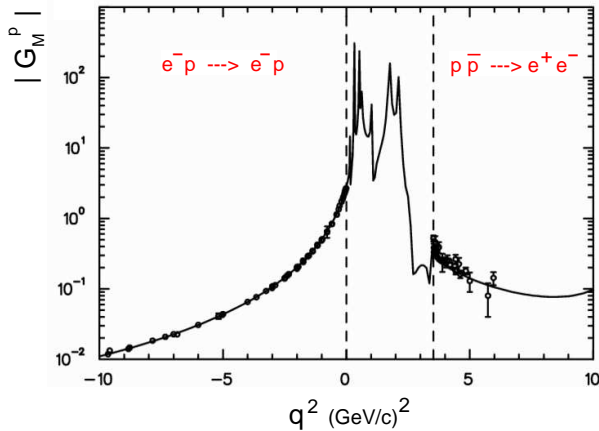


**Figure 1.** Experimental data and predictions for the magnetic proton form factor in the domain  $-10 \text{ GeV}^2/c^2 \leq q^2 \leq 10 \text{ GeV}^2/c^2$ . The figure is taken from [6].

invariant mass squared  $q^2 = s_{\bar{p}p}$  smaller than  $4m^2$ . The main purpose of our paper is to explore this possibility, which may give access to the proton form factors in the underthreshold region, for an off-shell nucleon. The idea to use a nucleus for that purpose was explored in the 80's using deuterium [12]. The reaction is then:

$$\bar{p}d \rightarrow e^+e^-n \quad (1)$$

(a crossed-channel of deuteron electrodisintegration). The aim of the present paper is to revive this study in view of the future antiproton facility FAIR at GSI.

Other channels can give access to the off-shell nucleon form factors in the timelike region, including the underthreshold region; such processes have been studied theoretically in ref. [13] ( $\gamma p \rightarrow pe^+e^-$ ) and in refs. [14,15] ( $\bar{p}p \rightarrow \pi^0 e^+e^-$ ).

The paper is organized as follows: a theoretical study is presented in sect. 2 and experimental aspects are presented in sect. 3. Other aspects are mentioned in sect. 4 and a conclusion is given in sect. 5.

## 2 Theoretical study

In elastic electron scattering from the nucleon  $e^-N \rightarrow e^-N$  the momentum transfer squared  $q^2 = (k - k')^2$  is always negative. This allows to measure the nucleon form factors in the space-like domain of  $q^2$ .

On the contrary, in the annihilation  $N\bar{N} \rightarrow \gamma^* \rightarrow e^+e^-$  the mass of virtual photon is equal to the total c.m.  $N\bar{N}$  energy. Its four-momentum squared is always greater than  $4m^2$ . This allows to measure the nucleon form factors in the time-like domain of  $q^2$ , above the  $N\bar{N}$  threshold. In this reaction, in order to study the form factor be-

havior in a narrow domain near threshold, where non-trivial structures are predicted [9], one should have a beam of almost stopped antiprotons. This non-easy technical problem was solved at LEAR [10]. However, the underthreshold domain  $0 \leq q^2 \leq 4m^2$  remains kinematically unreachable in this type of experiments.

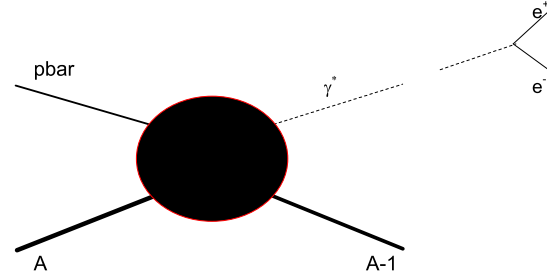


**Figure 2.** The process  $\bar{p}A \rightarrow (A-1)\gamma^*$  (followed by  $\gamma^* \rightarrow e^+e^-$ ).

One can penetrate in this domain of  $q^2$  in the  $\bar{p}$  annihilation on nuclei

$$\bar{p}A \rightarrow (A-1)e^+e^-,$$

see fig. 2. The symbol  $(A-1)$  means not necessarily a nucleus but any system with the baryon number  $A-1$ . Since extra energy of the antiproton can be absorbed by the  $(A-1)$  system, the  $e^+e^-$  pair may be emitted with very small invariant mass. Therefore the two-body reaction  $\bar{p}A \rightarrow (A-1)\gamma^*$  is kinematically allowed for a very wide domain of invariant mass of the  $\gamma^*$ , which starts with two times the electron mass, namely:

$$4m_e^2 \leq q^2 \leq (\sqrt{s_{\bar{p}A}} - M_{A-1})^2.$$

One can achieve near-threshold, under-threshold and even deep-under-threshold values of  $q^2$  even for fast antiprotons. This however does not mean that this reaction provides us direct information about the nucleon form factors. For the latter, we should be sure that the observed  $e^+e^-$  pair (and nothing more) was created in the annihilation  $\bar{p}p \rightarrow e^+e^-$  on the proton in the nucleus, i.e., that the reaction mechanism is given by the diagram of fig. 3 or by a similar diagram where the  $\bar{p}$  can rescatter before annihilation.

At the same time, since the nucleons in the nucleus are off-mass-shell, the form factors entering the amplitude of fig. 3, are not precisely the same as found in the free  $\bar{p}p$  annihilation. In general, the three-leg vertex, shown in fig. 4, depends not only on the photon virtuality  $q^2$ ,

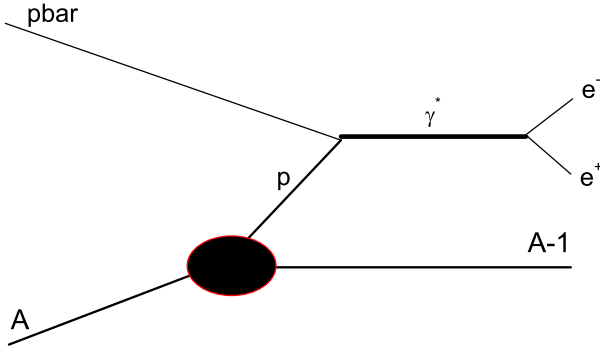


**Figure 3.** Amplitude of the reaction  $\bar{p}A \rightarrow (A-1)\gamma^*$  in impulse approximation.

but also on the nucleon ones  $p_1^2, p_2^2$ :  $F = F(p_1^2, p_2^2, q^2)$ . In the case considered, the incident antiproton is on-energy-shell:  $p_{\bar{p}}^2 = m^2$ , however the form factors depend on the proton virtuality  $p_p^2$ . How the form factor  $F(p_{\bar{p}}^2 = m^2, p_p^2 \neq m^2, q^2)$  v.s.  $q^2$  differs from the free one  $F(p_{\bar{p}}^2 = m^2, p_p^2 = m^2, q^2)$  – this depends on the dynamics determining its behavior v.s. the nucleon leg virtuality. The nucleon form factors with off-shell nucleons were studied in the papers [16,17]. When only one nucleon is off-shell, then there are six form factors instead of two in the on-shell case. Generally, we can expect that the form factor dependence v.s.  $p_p^2$  is much smoother than the  $q^2$  dependence. The  $p_p^2$  dependence can be determined by the nucleon self-energy corrections (i.e., by the structure of the nucleon), whereas the  $q^2$  dependence in the time-like domain is governed by the  $\bar{p}p$  interaction. The nucleon dynamics has a much larger energy scale than the nuclear one. The typical off-shell variation found in the papers [16,17] was from a few to 10 percent. We do not pretend to such an accuracy here. Therefore we neglect this effect in our calculation. We will come to this question later. In any case, both domains:  $q^2 < 4m^2$ ,  $p_p^2 = m^2$  and  $q^2 < 4m^2$ ,  $p_p^2 < m^2$  are totally unexplored experimentally and are interesting and intriguing.

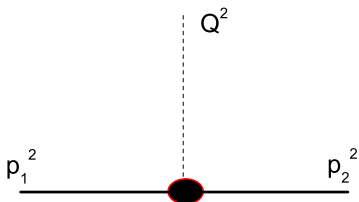


**Figure 4.** Nucleon electromagnetic vertex.

We emphasize that though the form factor dependence on  $p_p^2$  can be weak, the nucleon off-mass-shell effect is very important for the kinematical possibility to reach the near- and under-threshold domain of  $q^2$  with fast antiprotons. To produce the near-threshold  $e^+e^-$  pairs in annihilation of a fast  $\bar{p}$  on an on-mass-shell proton, the antiproton should meet in the nucleus a fast proton with parallel momentum. The probability of that, which we estimated in the Glauber approach, is negligibly small [18] relative to the results presented below. However, if the effective mass  $p_p^2$  of the virtual proton is smaller than  $m^2$  (that is just the case in a nucleus), then the near- and under-threshold  $e^+e^-$  pairs can be produced in collisions with not so fast intra-nucleus nucleons. This effect considerably increases the cross section. To have an idea of the order of magnitude which one can expect for this cross section, we will calculate it in the impulse approximation. Numerical applications will be done for the lowest antiproton beam momentum foreseen in future projects. Namely, at the High Energy Storage Ring at FAIR-GSI this value is 1.5 GeV/c.

## 2.1 Cross section calculation

At first, we consider the case of the deuteron target. If we know the amplitude of the reaction  $\bar{p}d \rightarrow e^+e^-n$ :  $M_{\bar{p}d \rightarrow e^+e^-n}$  (to be calculated below), then the corresponding cross section is given by:

$$d\sigma_{\bar{p}d \rightarrow e^+e^-n} = \frac{(2\pi)^4}{4I} |M_{\bar{p}d \rightarrow e^+e^-n}|^2 \times \delta^{(4)}(p_{\bar{p}} + p_d - p_{e^+} - p_{e^-} - p_n) \times \frac{d^3 p_{e^+}}{(2\pi)^3 2\epsilon_{e^+}} \frac{d^3 p_{e^-}}{(2\pi)^3 2\epsilon_{e^-}} \frac{d^3 p_n}{(2\pi)^3 2\epsilon_n} \quad (2)$$

where  $I$  results from the flux factors:

$I = j_{\bar{p}} \epsilon_d = [(p_{\bar{p}} \cdot p_d)^2 - m^2 M_d^2]^{1/2} = M_d p_{\bar{p},lab} \approx 2m p_{\bar{p},lab}$ ,  $p_{\bar{p},lab}$  is the incident  $\bar{p}$  momentum in the lab. system. Here and below we imply the sum over the final spin projections and average over the initial ones.

We are interested in the distribution in the invariant mass  $\mathcal{M}$  of the final  $e^+e^-$  system. To find it, for fixed value of  $\mathcal{M}$ , we can integrate, in some limits, over the angles of the recoil neutron (determining the neutron recoil momentum) and over the angles of the emitted  $e^+e^-$  in their center of mass. This can be done using standard techniques of the phase volume transformations. Namely, we use the identity:

$$\int \delta^{(4)}(\mathcal{P}_{e^+e^-} - p_{e^+} - p_{e^-}) d^4 \mathcal{P}_{e^+e^-} \delta(\mathcal{P}_{e^+e^-}^2 - \mathcal{M}^2) d\mathcal{M}^2 \equiv 1,$$

where  $\mathcal{P}_{e^+e^-}$  is the four-momentum of the  $e^+e^-$  pair and  $\mathcal{M}^2$  is its invariant mass squared. We insert this formula

in the cross section (2) and represent the three-body phase volume in (2) as:

$$\begin{aligned} d\sigma_{\bar{p}d \rightarrow e^+e^-n} &= \int \dots \delta^{(4)}(p_{\bar{p}} + p_d - p_{e^+} - p_{e^-} - p_n) \\ &\times \frac{d^3 p_{e^+}}{2\epsilon_{e^+}} \frac{d^3 p_{e^-}}{2\epsilon_{e^-}} \frac{d^3 p_n}{2\epsilon_n} \\ &= \int \dots \delta^{(4)}(p_{\bar{p}} + p_d - \mathcal{P}_{e^+e^-} - p_n) \\ &\times \delta^{(4)}(\mathcal{P}_{e^+e^-} - p_{e^+} - p_{e^-}) d^4 \mathcal{P}_{e^+e^-} \delta(\mathcal{P}_{e^+e^-}^2 - \mathcal{M}^2) d\mathcal{M}^2 \\ &\times \frac{d^3 p_n}{2\epsilon_n} \frac{d^3 p_{e^+}}{2\epsilon_{e^+}} \frac{d^3 p_{e^-}}{2\epsilon_{e^-}} = \int \dots dV_1 dV_2 d\mathcal{M}^2 \end{aligned}$$

where  $\epsilon_n$  is the energy corresponding to the four-momentum  $p_n$  and similarly for other energies, and we give explicitly only the factors resulting from the phase volume. We denoted the phase volume of the  $e^+e^-$  pair as:

$$\begin{aligned} dV_1 &= \int \delta^{(4)}(\mathcal{P}_{e^+e^-} - p_{e^+} - p_{e^-}) \frac{d^3 p_{e^-}}{2\epsilon_{e^-}} \frac{d^3 p_{e^+}}{2\epsilon_{e^+}} \\ &= \frac{p_e^*}{4\mathcal{M}} d\Omega_e \approx \frac{1}{8} d\Omega_e. \end{aligned} \quad (3)$$

Here  $p_e^*$  is the final electron (or positron) momentum in the c.m. frame of the  $e^+e^-$  pair and  $\Omega_e$  is its solid angle in this frame. Neglecting the electron mass, we replaced:  $p_e^* \approx \frac{1}{2}\mathcal{M}$ .

The two-body phase volume  $dV_2$  of the final  $n\gamma^*$  state reads:

$$\begin{aligned} dV_2 &= \int \delta^{(4)}(p_{\bar{p}} + p_d - \mathcal{P}_{e^+e^-} - p_n) \frac{d^3 \mathcal{P}_{e^+e^-}}{2\epsilon_{\mathcal{M}}} \frac{d^3 p_n}{2\epsilon_n} \\ &= \frac{p_{\gamma^*n}^*}{4\sqrt{s_{\bar{p}d}}} d\Omega_{\gamma^*n}^*. \end{aligned} \quad (4)$$

Here  $p_{\gamma^*n}^*$  and  $\Omega_{\gamma^*n}^*$  are in the c.m. frame of the reaction (i.e., the c.m. frame of  $\bar{p}d$ ) and  $s_{\bar{p}d}$  is the corresponding c.m. energy squared.

In this way we obtain

$$d\sigma_{\bar{p}d \rightarrow e^+e^-n} = \frac{1}{2^8 \pi^5 m p_{\bar{p},lab}} \int |M_{\bar{p}d \rightarrow e^+e^-n}|^2 dV_1 dV_2 d\mathcal{M}^2. \quad (5)$$

This form of the cross section will provide us the invariant mass distribution  $d\sigma_{\bar{p}d \rightarrow e^+e^-n}/d\mathcal{M}$ .

The formula (5) is general and does not assume any particular mechanism of the reaction. In the impulse approximation, when the mechanism is given by the diagram of fig. 3, the total amplitude squared  $|M_{\bar{p}d \rightarrow e^+e^-n}|^2$  is proportional to the annihilation amplitude squared  $|M_{\bar{p}p \rightarrow e^+e^-}|^2$  and to the square of the deuteron wave function  $|\psi|^2$ . The direct calculation of the amplitude corresponding to the diagram of fig. 3 gives the proportionality coefficient:

$$|M_{\bar{p}d \rightarrow e^+e^-n}|^2 = 4m |M_{\bar{p}p \rightarrow e^+e^-}|^2 |\psi|^2, \quad (6)$$

and  $|\psi|^2$  is normalized as:

$$\int |\psi(k)|^2 \frac{md^3k}{(2\pi)^3 \epsilon_k} = 1. \quad (7)$$

Substituting (6) into (5), we find the cross section:

$$\begin{aligned} d\sigma_{\bar{p}d \rightarrow e^+e^-n} &= \frac{1}{2^6 \pi^5 p_{\bar{p},lab}} \int |M_{\bar{p}p \rightarrow e^+e^-}|^2 \frac{1}{8} d\Omega_e \\ &\times |\psi|^2 \frac{p_{\gamma^*n}^*}{4\sqrt{s_{\bar{p}d}}} d\Omega_{\gamma^*n}^* d\mathcal{M}^2. \end{aligned}$$

We integrate over  $d\Omega_e$  (in the  $e^+e^-$  c.m. system) and finally obtain:

$$\frac{d\sigma_{\bar{p}d \rightarrow e^+e^-n}}{d\mathcal{M}} = \sigma_{\bar{p}p \rightarrow e^+e^-}(\mathcal{M}) \eta(\mathcal{M}), \quad (8)$$

where  $\eta(\mathcal{M})$  is the distribution (given by eq. (11) below) of the  $e^+e^-$  invariant mass  $\mathcal{M}$  due to the fact that the reaction occurs on the proton bound in the nucleus, and  $\sigma_{\bar{p}p \rightarrow e^+e^-}(\mathcal{M})$  is the cross section of the  $\bar{p}p \rightarrow e^+e^-$  annihilation at the total energy  $\mathcal{M}$ . The latter is determined by the amplitude  $M_{\bar{p}p \rightarrow e^+e^-}$ , corresponding to annihilation via the  $s$ -channel photon  $\gamma^*$ . The calculation of this amplitude is standard. Though the target proton is off-mass-shell, we do not consider the off-mass-shell effects in this amplitude, i.e. we assume a free proton. Then the amplitude squared reads:

$$\begin{aligned} |M_{\bar{p}p \rightarrow e^+e^-}|^2 &= \frac{16\alpha^2 \pi^2}{\mathcal{M}^2} \cdot [4m^2 |G_E|^2 \sin^2 \theta_{e^+} \\ &+ \mathcal{M}^2 |G_M|^2 \cos^2 \theta_{e^+}], \end{aligned} \quad (9)$$

where  $\theta_{e^+}$  is the emission angle of the  $e^+$  or the  $e^-$  in the  $\gamma^*$  c.m. frame and  $G_E, G_M$  are the proton electric and magnetic timelike form factors. To estimate the nuclear effect, from now on we omit the form factors, i.e. we put  $|G_E| = |G_M| = 1$ , or  $|F_1| = 1, |F_2| = 0$  as for a pointlike nucleon. Then the  $\bar{p}p \rightarrow e^+e^-$  cross section obtains the form:

$$\begin{aligned} \sigma_{\bar{p}p \rightarrow e^+e^-} &= \frac{1}{64\pi^2} \frac{p_e^*}{m p_{\bar{p},lab} \mathcal{M}} \int |M_{\bar{p}p \rightarrow e^+e^-}|^2 d\Omega_e \\ &= \frac{2\alpha^2 \pi (2m^2 + \mathcal{M}^2)}{3\mathcal{M}^2 m p_{\bar{p},lab}}. \end{aligned} \quad (10)$$

Though  $\sigma_{\bar{p}p \rightarrow e^+e^-}$  depends on  $\mathcal{M}$ , the main (nuclear) effect is determined by the factor  $\eta(\mathcal{M})$ :

$$\eta(\mathcal{M}) = \frac{m p_{\gamma^*n}^* \mathcal{M}}{(2\pi)^2 \sqrt{s_{\bar{p}d}}} \int_{-1}^1 |\psi(k)|^2 dz. \quad (11)$$

Here  $z = \cos \theta$ , where  $\theta$  is the angle, in the c.m. frame of the reaction, between the initial deuteron momentum

$p_d^*$  and the final neutron momentum  $p_n^*$ . The integration over  $dz$  in  $\eta(\mathcal{M})$  results from  $d\Omega_{\gamma^*n}$  in the phase volume  $dV_2$ , eq. (4). The argument of the wave function  $k$  depends on  $z$ . This explicit dependence is given in the next section.

The distribution  $\eta(\mathcal{M})$  is normalized to 1:

$$\int_0^\infty \eta(\mathcal{M}) d\mathcal{M} = 1. \quad (12)$$

To prove eq. (12), we calculate this integral explicitly:

$$\int_0^\infty \eta(\mathcal{M}) d\mathcal{M} = \int |\psi(k)|^2 \frac{mp_{\gamma^*n}^* \mathcal{M}}{(2\pi)^2 \sqrt{s_{\bar{p}d}}} d\mathcal{M} \sin\theta d\theta \frac{d\phi}{2\pi}.$$

Since

$$\epsilon_n^* = (s_{\bar{p}d} - \mathcal{M}^2 + m^2) / (2\sqrt{s_{\bar{p}d}}), \quad (13)$$

we have:  $\mathcal{M} d\mathcal{M} = -\sqrt{s_{\bar{p}d}} d\epsilon_n^*$ . Then:  $d\epsilon_n^* = \frac{p_n^* d p_n^*}{\epsilon_n^*}$ . In this way we find:

$$\begin{aligned} \int \eta(\mathcal{M}) d\mathcal{M} &= \int |\psi(k)|^2 \frac{mp_n^{*2} d p_n^*}{(2\pi)^3 \epsilon_n^*} d\Omega^* \\ &= \int |\psi(k)|^2 \frac{md^3k}{(2\pi)^3 \epsilon_k} = 1. \end{aligned}$$

The latter equality is just the normalization condition (7) of the wave function. Here the neutron momentum  $p_n^*$  is defined in the c.m. frame of the total reaction, whereas the momentum  $k$  is defined in the c.m. frame of the  $np$  system. So,  $p_n^*$  and  $k$  are the momentum of the same particle, but in different frames. We replaced  $mp_n^{*2} d p_n^* d\Omega^* / \epsilon_{p_n^*}$  by  $\frac{md^3k}{\epsilon_k}$ , since this integration volume is a relativistic invariant.

The total cross section is obtained by integrating (8) in the finite limits  $\mathcal{M}_{min} \leq \mathcal{M} \leq \mathcal{M}_{max}$ , where  $\mathcal{M}_{min} = 2m_e$ ,  $\mathcal{M}_{max} = \sqrt{s_{\bar{p}d}} - m$ . Neglecting the electron mass, we can put  $\mathcal{M}_{min} = 0$ . For  $p_{\bar{p},lab} = 1.5$  GeV/c the value  $\mathcal{M}_{max}$  is high enough and provides the normalization condition (12) with very high accuracy.

To emphasize more distinctly the effect of the nuclear target, we can represent the cross section (10) of the annihilation  $\bar{p}p \rightarrow e^+e^-$  on a free proton similarly to eq. (8):

$$\frac{d\sigma_{\bar{p}p \rightarrow e^+e^-}}{d\mathcal{M}} = \sigma_{\bar{p}p \rightarrow e^+e^-} \delta(\mathcal{M} - \sqrt{s_{p\bar{p}}}) \quad (14)$$

where  $\sigma_{\bar{p}p \rightarrow e^+e^-}$  is defined in (10),  $s_{p\bar{p}} = (p_p + p_{\bar{p}})^2 = 2m^2 + 2m\sqrt{p_{\bar{p},lab}^2 + m^2}$ .

The fact that in the annihilation on a free proton the mass of the final  $e^+e^-$  pair is fixed is reflected in (14) in the presence of the delta-function. Comparing this formula with (8), we see that the effect of the nuclear target results in a dilation of the infinitely sharp distribution  $\delta(\mathcal{M} - \sqrt{s_{p\bar{p}}})$  in a distribution of finite width  $\eta(\mathcal{M})$ . The

dilation of a distribution does not change its normalization:  $\eta(\mathcal{M})$  remains normalized to 1.

For a test of calculation we can find from (9) (or extract from (10)) the amplitude squared  $|\overline{M_{\bar{p}p \rightarrow e^+e^-}}|^2$ , averaged over the angle  $\theta_{e^+}$ :

$$\overline{|M_{\bar{p}p \rightarrow e^+e^-}|^2} = \frac{64\pi^2 \alpha^2 (\mathcal{M}^2 + 2m^2)}{3\mathcal{M}^2}$$

Due to time invariance, it is equal to  $|\overline{M_{e^+e^- \rightarrow \bar{p}p}}|^2$ . Then we can identify  $m$  with the muon mass and find the total cross section of the reaction  $e^+e^- \rightarrow \mu^+\mu^-$ :

$$\sigma_{e^+e^- \rightarrow \mu^+\mu^-} = \frac{p^* \overline{|M_{e^+e^- \rightarrow \mu^+\mu^-}|^2}}{64\pi E^{*3}},$$

( $p^*$  and  $E^*$  are the final muon momentum and energy). It coincides with a well-known result and, at high  $e^+e^-$  energy, turns into  $\sigma_{e^+e^- \rightarrow \mu^+\mu^-} = \frac{4\pi\alpha^2}{3s_{e^+e^-}}$  given in textbooks. This confirms the correctness of numerous factors appearing in our formulas.

## 2.2 Analysis and numerical calculations

So far we have not defined the argument  $k$  in the wave function  $\psi(k)$  determining the distribution (11). The integral over  $dz$  incorporates an interval of  $k$ , which, as we will see, for  $p_{\bar{p}} = 1500$  MeV/c and  $\mathcal{M} = 2m$  starts with the minimal value  $k_{min} \approx 360$  MeV/c. For these values the relativistic effects become non-negligible, therefore different relativistic approaches result, in principle, in different expressions for  $k$ . If we take as the argument the spectator momentum (the momentum of the neutron) in the rest frame of the deuteron, then it is expressed as:  $k^2 = \epsilon_n^2 - m^2$ , where the neutron lab. energy can be represented as  $\epsilon_n = (p_d \cdot p_n) / M_d$ , so that when  $p_d = (M_d, \mathbf{0})$  we obtain identity. Introducing the invariant  $t = (p_d - p_n)^2$ , and since  $p_d \cdot p_n = (M_d^2 + m^2 - t) / 2$ , we get:

$$k^2 = \frac{(M_d^2 + m^2 - t)^2}{4M_d^2} - m^2. \quad (15)$$

In the c.m. frame of the total reaction  $\bar{p}d \rightarrow e^+e^-n$ , the variable  $t$  is expressed as:

$$t = (p_d - p_n)^2 = M_d^2 - 2(\epsilon_d^* \epsilon_n^* - z p_d^* p_n^*) + m^2 \quad (16)$$

where  $\epsilon_d^*$ ,  $\epsilon_n^*$  and  $p_d^*$ ,  $p_n^*$  are the c.m. energies and momenta of the deuteron and the neutron,  $z = \cos\theta$  and  $\theta$ , as already mentioned, is the angle between  $p_d^*$  and  $p_n^*$ . The energy  $\epsilon_n^*$  is given by eq. (13), whereas  $\epsilon_d^*$  is obtained from (13) by the replacement of  $\mathcal{M}^2$  by  $M_d^2$ . After these precisions, the formula (15) together with (16) completely determines the argument of the wave function.

It should also be emphasized that the proton is off-mass-shell. Its off-shell mass squared has the value  $(m^*)^2 = p_p^2 = t$ , which depends on kinematics.

The minimal value  $k_{\min}$  is achieved at  $z = 1$ , i.e. when the neutron recoils antiparallel to the incident antiproton. Using eqs.(15) and (16), one finds a value that is remarkably small:  $k_{\min} \approx 360$  MeV/c, corresponding to an off-shell mass  $m^* \approx 800$  MeV ( $\approx 0.85m$ ) for the initial proton.

We emphasize the meaning of the integration over  $z$  in eq. (11). The incident antiproton with momentum  $\mathbf{p}_{\bar{p}}^*$  in the  $\bar{p}d$  c.m. frame meets in the deuteron the proton with momentum  $\mathbf{p}_p^*$ . In the impulse approximation (diagram of fig. 3), the latter is determined by the difference of the deuteron and the neutron momenta:  $\mathbf{p}_p^* = \mathbf{p}_d^* - \mathbf{p}_n^*$ . Since eq. (11) gives the value of  $\eta(\mathcal{M})$  at fixed  $\mathcal{M}$ , for all these momenta and the relative angles between them and for the virtual proton mass squared  $(m^*)^2 = t$ , the invariant energy  $\sqrt{s_{p\bar{p}}} = \sqrt{(p_p + p_{\bar{p}})^2}$  is just equal to the given invariant mass  $\mathcal{M}$  of the virtual  $\gamma^*$  and of the final  $e^+e^-$  pair. In this way, we obtain the contribution of the events with given time-like value of  $q^2 = \mathcal{M}^2$  in the cross section. When the angle  $\theta$  between  $\mathbf{p}_n^*$  and  $\mathbf{p}_d^*$  (and  $z = \cos \theta$ ) varies, the modulus of the proton momentum, its direction and the off-shell mass  $m^*$  vary correspondingly to provide the same fixed value of  $s_{p\bar{p}} = \mathcal{M}^2 = q^2$ . The integral over  $z$  in (11) incorporates all these events, with different  $\mathbf{p}_p^*$ ,  $m^*$  and with the same  $q^2$ .

At first glance, the small near-threshold  $\bar{p}p$  c.m. energy  $\mathcal{M} \approx 2m$  in the collision of a fast  $\bar{p}$  ( $p_{\bar{p}} = 1500$  MeV/c) is achieved, when the antiproton meets in the deuteron a fast proton having the same momentum as the  $\bar{p}$ , in modulus and direction. The protons with such a high momentum are very seldom in deuteron. For this mechanism, the cross section would be very small. However, the near-threshold value of  $\mathcal{M}$  is obtained in other kinematics. As we mentioned, the proton momenta  $k$  in the deuteron wave function  $\psi(k)$  in eq. (11) start with  $k \approx k_{\min} \approx 360$  MeV/c only (that corresponds to  $z \approx 1$ ). The main reason which allows to obtain in this collision the value  $\mathcal{M} \approx 2m$  is the off-shellness of the proton:  $m^* \leq 0.85m$  instead of  $m^* = m$ . This 15% decrease relative to the free proton mass is enough to obtain the invariant  $\bar{p}p$  mass  $\mathcal{M} \approx 2m$ , when one has the two parallel momenta: 1500 MeV/c for  $\bar{p}$  and 360 MeV/c for  $p$ .

We also notice that for other values of  $z$ , i.e. non-colinear  $p$  and  $\bar{p}$  momenta, the proton momentum  $k$  needed to produce  $\mathcal{M} \approx 2m$  is larger than  $k_{\min}$ . In a correlated way, this proton is also further away from the mass-shell.

The calculation in the framework of another relativistic approach – light-front dynamics [19] – gives another formula for  $k$  which numerically is very close to the one

of eq.(15), reducing the minimal value  $k_{\min}$  by 10 MeV/c only.

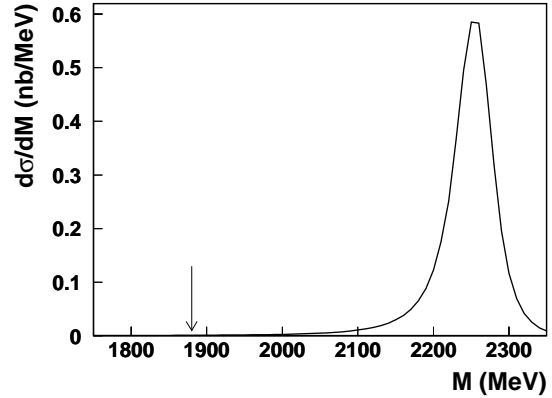


**Figure 5.** The cross section  $\frac{d\sigma_{\bar{p}d \rightarrow e^+e^-n}}{d\mathcal{M}}$  of the reaction  $\bar{p}d \rightarrow e^+e^-n$  v.s.  $\mathcal{M}$ , in the interval:  $1750 \text{ MeV} \leq \mathcal{M} \leq 2350 \text{ MeV}$ , calculated for a pointlike proton. The arrow indicates the  $\bar{p}p$  threshold.

The cross section  $d\sigma_{\bar{p}d \rightarrow e^+e^-n}/d\mathcal{M}$ , eq. (8), has been calculated for an antiproton of momentum  $p_{\bar{p}} = 1500$  MeV/c on a deuteron nucleus at rest, with the deuteron wave function [20], incorporating two components corresponding to S- and D-waves. The result is shown in fig. 5. The maximum of the cross section is at  $\mathcal{M} = 2257$  MeV, that corresponds to the  $\bar{p}$  interacting with a proton at rest (and on-shell). The cross section integrated over  $\mathcal{M}$  is equal to 43 nb. We remind that these calculations do not take into account the proton form factor. Its influence will be estimated below. The numerical integral over  $\mathcal{M}$  of the function  $\eta(\mathcal{M})$ , eq. (11), is  $\approx 1$ , in accordance with the normalization condition (12).

The  $\bar{p}p$  threshold value  $\mathcal{M} = 1880$  MeV is on the tail of the distribution, far from the maximum. Relative to the maximum, the cross section at threshold decreases approximately by a factor 600. The numerical value at the threshold is:

$$\left. \frac{d\sigma}{d\mathcal{M}} \right|_{\mathcal{M}=2m} = 1 \frac{pb}{\text{MeV}}. \quad (17)$$

In fig. 6 this cross section is shown in the near-threshold interval  $1830 \text{ MeV} \leq \mathcal{M} \leq 1930 \text{ MeV}$ . The integral over  $\mathcal{M}$  in a bin of width 100 MeV centered on the threshold is:

$$\int_{1830 \text{ MeV}}^{1930 \text{ MeV}} \frac{d\sigma_{\bar{p}d \rightarrow e^+e^-n}}{d\mathcal{M}} d\mathcal{M} \approx 100 \text{ pb}.$$

These estimations take into account the suppression resulting from the momentum distribution in deuteron. However, they do not incorporate the form factors of the

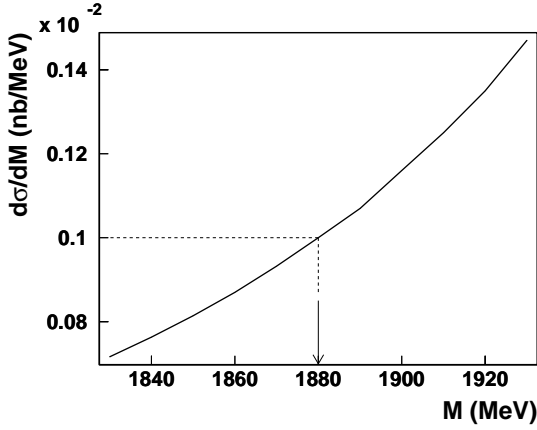


**Figure 6.** The same as in fig. 5, but near the  $p\bar{p}$  threshold, in the interval  $1830 \text{ MeV} \leq \mathcal{M} \leq 1930 \text{ MeV}$ .

nucleon. To incorporate them in a simplified way, one can consider an effective form factor  $|F|$  which depends on  $\mathcal{M}$ , and include it in the integral:

$$\sigma_{\bar{p}d \rightarrow e^+e^-n} = \int \sigma_{\bar{p}p \rightarrow e^+e^-}(\mathcal{M}) \eta(\mathcal{M}) |F(\mathcal{M})|^2 d\mathcal{M} \quad (18)$$

where  $\sigma_{\bar{p}p \rightarrow e^+e^-}(\mathcal{M})$  is the cross section for pointlike nucleons given in eq.(10). To have an estimate of this integral, we have taken the effective proton form factor measured in ref. [11]. By doing this, we neglect all off-shell effects. We interpolate  $|F(\mathcal{M})|$  linearly between the measured values, and we limit the integral to the region  $\mathcal{M} \geq 2m$ . In this way we obtain  $\sigma_{\bar{p}d \rightarrow e^+e^-n} \simeq 1 \text{ nb}$ , which is comparable to the total cross section  $\sigma_{\bar{p}p \rightarrow e^+e^-}$  on a free proton at  $\mathcal{M} = 2257 \text{ MeV}$ .<sup>1</sup>

Figure 7 shows the integrand of eq.( 18) as a function of  $\mathcal{M}$ , using the above choice of form factor. One notices the rapid rise of the cross section as  $\mathcal{M}$  approaches the  $p\bar{p}$  threshold. Lastly, we point out that at threshold, our differential cross section  $d\sigma_{\bar{p}d \rightarrow e^+e^-n}$  of  $1 \text{ pb/MeV}$  (eq.(17)) is not suppressed by any factor, since there the form factor  $|F|$  seems to be close to 1 experimentally [21,22]. Below this threshold one may expect a form factor effect *larger* than one, but this is not known and this is the goal of the proposed study.

<sup>1</sup> This cross section  $\sigma_{\bar{p}p \rightarrow e^+e^-} = 1 \text{ nb}$  at  $\mathcal{M} = 2257 \text{ MeV}$  is obtained from the measured cross section  $\sigma_{e^+e^- \rightarrow \bar{p}p}$  at the same c.m. energy, which we estimate to be  $\simeq 318 \text{ pb}$ , from interpolation in the data of ref. [11]. This value is then multiplied by the factor  $\mathcal{M}^2/(\mathcal{M}^2 - 4m^2) \approx 3.27$  to obtain the cross section in the inverse channel  $\bar{p}p \rightarrow e^+e^-$  at the same c.m. energy.

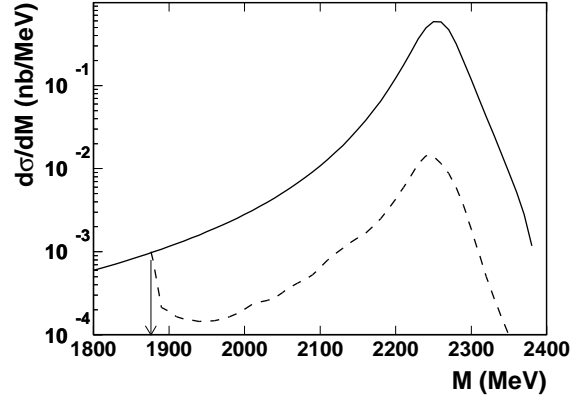


**Figure 7.** The cross section  $\frac{d\sigma_{\bar{p}d \rightarrow e^+e^-n}}{d\mathcal{M}}$  including an effective form factor (see text) is drawn as a dashed curve above the  $p\bar{p}$  threshold. The solid curve is the same as in fig. 5 (but now in logarithmic scale).

### 2.3 Annihilation on heavier nuclei

For  $A > 2$ , we should take into account the possibility of excitation and breakup of the final nucleus  $A - 1$  in the process  $\bar{p}A \rightarrow (A - 1)\gamma^*$ . The result contains the sum over the final energies of the residual nucleus and the integral over a continuous spectrum. That is, the function  $|\psi(k)|^2$  in eq. (11) is replaced by the integral  $\int_{E_{min}}^{E_{max}} S(E, k) dE$ , where  $S(E, k)$  is the nucleus spectral function giving the probability to find in the final state the nucleon with the relative momentum  $k$  and the residual nucleus with energy  $E$ . For high incident energy we can replace the upper limit by infinity. Then we obtain:

$$\int_{E_{min}}^{\infty} S(E, k) dE = n(k),$$

where  $n(k)$  is the momentum distribution in the nucleus.

To estimate the cross section on heavy nuclei, we will still use eqs. (8), (11) but with the two following changes. (i) We replace the deuteron momentum distribution by the nuclear one. Since the deuteron wave function is normalized by (7), whereas  $n(k)$  is usually normalized as  $\int n(k) d^3k = 1$ , we replace  $\psi^2(k)$  in (11) by  $(2\pi)^3 \epsilon_k n(k) / m$ . (ii) We multiply (11) by the number of protons  $Z$ .

The numerical calculations were carried out for the  $^{12}\text{C}$ ,  $^{56}\text{Fe}$  and  $^{197}\text{Au}$  nuclei with the nuclear momentum distributions found in the papers [23,24]. Near threshold, i.e. at  $\mathcal{M} = 1880 \text{ MeV}$ , for all three nuclei we obtain very close results given by:

$$\frac{d\sigma_{\bar{p}A \rightarrow e^+e^-X}}{d\mathcal{M}} \approx 6.5 Z \frac{\text{pb}}{\text{MeV}} \quad (19)$$

Multiplying by the charge  $Z$  ( $Z(^{12}\text{C}) = 6$ ,  $Z(^{56}\text{Fe}) = 26$ ,  $Z(^{197}\text{Au}) = 79$ ) and integrating (19) over a 1 MeV interval near  $\mathcal{M} = 1880$  MeV, we get:

$$\sigma(^{12}\text{C}) = 39 \text{ pb}, \quad \sigma(^{56}\text{Fe}) = 0.17 \text{ nb}, \quad \sigma(^{197}\text{Au}) = 0.5 \text{ nb}.$$

These results were found without taking into account the absorption of  $\bar{p}$  in nucleus before electromagnetic annihilation. This absorption was estimated in Glauber approach (it is applicable since now we do not need high nucleon momenta). It reduces these cross sections by only a factor 2. We recall again that these results are obtained for structureless nucleons.

## 2.4 Beyond the impulse approximation

Without carrying out any calculation, we discuss in this section other possible mechanisms for the process  $\bar{p}d \rightarrow e^+e^-n$ . One of them is the initial state interaction, which includes rescattering (not only elastic) of the initial  $\bar{p}$  in the target nucleus. In the rescattering, the incident  $\bar{p}$  loses energy and therefore the proton momentum needed to form the invariant mass  $\mathcal{M} \approx 2m$  becomes smaller. The probability to find such a proton in deuteron is higher. Therefore initial state interaction increases the cross section.

Though, if the rescattering is inelastic (with pion creation), it results in the reaction  $\bar{p}d \rightarrow e^+e^-N\pi$ . In this reaction, the  $e^+e^-$  pair is still produced in the  $\bar{p}p$  electromagnetic annihilation, giving an information about the proton timelike form factors. Therefore this process is also interesting in itself, although it is not in the scope of the paper.

Another mechanism of the reaction  $\bar{p}d \rightarrow e^+e^-n$  may include also the transition  $\bar{p}p \rightarrow \bar{n}n$  with the subsequent annihilation  $\bar{n}n \rightarrow e^+e^-$ . This transition can take place, for example, via meson exchange:

$$\begin{aligned} \bar{p}p &\rightarrow (\bar{n}\pi^-)p \rightarrow \bar{n}(\pi^-p) \rightarrow \bar{n}n, \\ \bar{p}p &\rightarrow \bar{p}(\pi^+n) \rightarrow (\bar{p}\pi^+)n \rightarrow \bar{n}n. \end{aligned}$$

If the annihilation  $\bar{n}n \rightarrow e^+e^-$  occurs on the same neutron which was created in the reaction  $\bar{p}p \rightarrow \bar{n}n$ , this does not give anything new, since this is simply a particular contribution  $\bar{p}p \rightarrow \bar{n}n \rightarrow e^+e^-$  in the initial state interaction incorporated in the full amplitude  $\bar{p}p \rightarrow e^+e^-$ , i.e., in the timelike proton form factor.

On the contrary, when the annihilation  $\bar{n}n \rightarrow \gamma^* \rightarrow e^+e^-$  occurs on another neutron (the neutron from deuteron), then the reaction  $\bar{p}d \rightarrow e^+e^-n$  gives information about the timelike neutron form factor. So, what is measured is the sum of two timelike form factors: the proton

and the neutron ones. One can expect that the direct annihilation  $\bar{p}p \rightarrow e^+e^-$  dominates over the mechanism with preliminary transition  $\bar{p}p \rightarrow \bar{n}n$ . In this case, the contribution of the proton form factor dominates.

We emphasize that in any case, whatever the intermediate steps are in process (1), the  $e^+e^-$  pair of the final state must come necessarily from the baryon-antibaryon electromagnetic annihilation,  $\bar{p}p$  or  $\bar{n}n$ , because there is only one neutron left at the end. It cannot come from another process, even if there are complicated intermediate steps, like rescattering, etc. Therefore this  $e^+e^-$  pair is a direct and very little distorted probe of the baryon-antibaryon electromagnetic annihilation vertex.

## 3 Experimental aspects

The aim of this section is to investigate the feasibility of process (1) in future experiments using antiproton beams. The study is made in the case of the  $\bar{\text{P}}\text{ANDA}$  experiment, which will use a state-of-the-art internal target detector at the High Energy Storage Ring (HESR) at FAIR-GSI. This study is only a first step, exploratory and rather qualitative. It remains to be pursued in more details in the future.

Regarding the target nucleus, we restrict ourselves to the deuteron. It is the only nucleus yielding a simple, three-body final state ( $e^+e^-n$ ), for which an experimental strategy can be defined. For heavier target nuclei  $A$ , the break-up channels will dominate over the three-body final state  $e^+e^- (A-1)$ , and no simple identification strategy can be defined. Indeed, to be able to use kinematical constraints in order to select the desired reaction, one needs to detect (at least) all final particles but one, a task which becomes more and more difficult as the number of nuclear fragments increases. As a side remark, we also note that the HESR luminosity in  $(\bar{p}A)$  decreases with the atomic charge  $Z$  of the target nucleus [25], in a way that roughly compensates the increase of cross section with  $Z$  reported in sect. 2.3.

New technologies for antiproton accelerators, targets and detectors provide a gain in luminosity and allow to access processes with very low cross sections, like the one presented here in the near-threshold region. In this section we first examine reaction (1) (the *signal*) and then the competing background processes. The presented material largely relies on the design performances of the  $\bar{\text{P}}\text{ANDA}$  detector [25,26] and the study of the electromagnetic process  $\bar{p}p \rightarrow e^+e^-$  on a free proton at rest [25,26,27].

### 3.1 Beam and target operating conditions

Considering the process  $\bar{p} + p_{\text{bound}} \rightarrow \gamma^*$  on an off-shell proton bound in the nucleus, the lower the antiproton beam momentum, the easier it is to reach a photon virtuality  $Q^2 < 4m^2$  ( $Q^2 = q^2$ ). Ideal conditions would be antiprotons of very low momentum. Here we consider the nominal lowest beam momentum that is foreseen in the HESR, i.e.  $p_{\bar{p},\text{lab}} = 1.5 \text{ GeV}/c$ . As seen in sect. 2.2, in these conditions only a very small fraction of the target protons in the deuteron will have enough off-shellness in order to produce a  $\bar{p}p$  system of invariant mass squared  $\leq 4m^2$ . In the impulse approximation, i.e. assuming that the neutron is a spectator in the  $\bar{p}d \rightarrow e^+e^-n$  process, these off-shell protons are found in the upper tail of the momentum distribution  $n(k)$  of the deuteron, at  $k = 360 \text{ MeV}/c$  and above.

In the  $\bar{\text{P}}\text{ANDA}$  experiment, nuclear targets will be used to study hadrons properties in the nuclear medium. For deuterium, an internal target of cluster-jet type or pellet type will be placed in the beam, and an effective target thickness of  $3.6 \cdot 10^{15} \text{ atoms}/\text{cm}^2$  is considered. At  $p_{\bar{p},\text{lab}} = 1.5 \text{ GeV}/c$ , beam losses limit the number of antiprotons to  $10^{11}$  per cycle, yielding a maximal value of  $5 \cdot 10^{31} \text{ cm}^{-2} \cdot \text{s}^{-1}$  for the cycle average luminosity  $\mathcal{L}$  in  $(\bar{p}d)$  collisions [25].

### 3.2 Count rate estimate for the process $\bar{p}d \rightarrow e^+e^-n$

With the above operating conditions ( $p_{\bar{p},\text{lab}}, \mathcal{L}$ ) and the cross section  $\sigma$  calculated in sect. 2.2, one can compute the number of events from process (1) in an ideal detector, covering the  $4\pi$  solid angle with 100 % efficiency; it is  $N = \mathcal{L} \cdot \sigma$ . For one month effective beamtime (i.e. corresponding to an integrated luminosity equal to  $\mathcal{L} \times 2.6 \cdot 10^6 \text{ s}$ ), this yields a large number of events integrated over the full range of dilepton invariant mass:  $N \sim 1.3 \times 10^5$  (this number is deduced from the cross section  $\sigma_{\bar{p}p \rightarrow e^+e^-} \sim 1 \text{ nb}$  on a free proton at rest). However, in the special region of interest near the  $N\bar{N}$  threshold, the cross section  $d\sigma/d\mathcal{M}$  is much reduced, of the order of  $1\text{pb}/\text{MeV}$  (see sect. 2.2), yielding a rate of 130 events per month in a 1 MeV bin of dilepton mass. This number of events is small, but other rare processes considered in the  $\bar{\text{P}}\text{ANDA}$  physics program have comparable expected rates.

On the one hand, the global detector efficiency and the necessary experimental cuts will reduce this amount of good events, with a reduction factor that could reach 50%. On the other hand, the cross section calculated in sect. 2.2 for process (1) is probably a lower limit in the subthreshold region, since there the proton form factor

can be larger than one and enhance the cross section. Therefore, all in all, within one month effective beamtime one could obtain an experimental spectrum of dilepton mass  $\mathcal{M}$  containing  $\sim$  a hundred signal events per MeV bin near the threshold ( $\mathcal{M} \sim 2m$ ). This would allow a first insight into possible structures in this region, including the totally unexplored subthreshold region.

### 3.3 Experimental signature of the exclusive channel $\bar{p}d \rightarrow e^+e^-n$ and related background processes

The selection of the exclusive reaction (1) is based on the detection of the lepton pair. The experimental strategy relies on three main characteristics of the detector: 1) its resolution, 2) its hermeticity and 3) its particle identification capability.

Regarding the first point, the main variable is the missing mass  $M_X$ , i.e. the invariant mass of the missing system  $X$  in the reaction  $\bar{p}d \rightarrow e^+e^-X$ . It is defined using the four-momentum vectors of the initial and detected particles:

$$M_X^2 = (p_{\bar{p}} + p_d - p_{e^+} - p_{e^-})^2.$$

Due to the many processes producing a lepton pair inclusively, this missing mass will have a wide distribution; for the events of reaction (1) a peak must be searched at the neutron mass, which represents the physical lower bound of the  $M_X$  spectrum. Therefore the experimental resolution in this missing mass is a crucial parameter (see sect. 3.4).

The background due to inclusive lepton pair production is quite large at the raw level. True  $e^+e^-$  pairs originate mostly from Dalitz decay (or direct  $l^+l^-$  decay) of mesons, and also from real photon conversion in the target. These types of processes will give dileptons mostly at low invariant mass ( $\mathcal{M} \leq 1 \text{ GeV}$ ), while we are looking for high-mass ones ( $\mathcal{M} \geq 1.8 \text{ GeV}$ ). Uncorrelated pairs coming from combinatorial background may form a high invariant mass; however they can be subtracted using the like-sign pairs (also combinatorial) as in heavy-ion dilepton experiments. All these processes of inclusive lepton pair production correspond to missing masses  $M_X$  larger than one neutron mass, and a large fraction of them can be eliminated by a proper cut in  $M_X$ . Also, these processes create more than three particles in the final state, and a condition on the observed particle multiplicity should be efficient to reject a large fraction of this background.

This brings us to the second important aspect, of detector hermeticity. The  $\bar{\text{P}}\text{ANDA}$  detector will cover almost the  $4\pi$  solid angle, by combining a target spectrometer for large polar angles and a forward spectrometer

for small angles. The good hermeticity is essential in the physics program in order to detect a complete spectrum of final states. In reaction (1) the neutron will go undetected most of the times; actually, in our kinematics of interest near threshold, this neutron is emitted at very backward angle w.r.t. the beam and will not hit any detector. With respect to hermeticity, potential background to reaction (1) consists in reactions in which, in addition to the  $e^+e^-$  pair, one or more light particles (pions, photons) are emitted and escape detection. They will contribute to form a missing system  $X$  (as defined above) of low baryonic mass, typically  $M_X \simeq m + m_\pi$ , polluting the region of interest. The simplest cases of such background reactions are:

$$\begin{aligned} \bar{p}d &\rightarrow e^+e^-n\pi^0 && (\text{from } \bar{p}p_{bound} \rightarrow \gamma^*\pi^0) \\ \bar{p}d &\rightarrow e^+e^-p\pi^- && (\text{from } \bar{p}n_{bound} \rightarrow \gamma^*\pi^-) \end{aligned}$$

on the bound proton or the bound neutron in the deuteron. The final  $\pi N$  state can be non-resonant or resonant (e.g. the  $\Delta(1232)$ ).

A third important aspect is the particle identification capability of the detector (PID), for charged and neutral particles. In  $\bar{P}$ ANDA, a global estimator [25] combines the information of the various subdetectors and will provide charged particle identification in the momentum range from 200 MeV/c to 10 GeV/c. In our case the most important task is to discriminate between  $e^\pm$  and  $\pi^\pm$ . Indeed, the main competing background to reaction (1) is of the type  $\bar{p}d \rightarrow \pi^+\pi^-n$  or  $\bar{p}d \rightarrow \pi^+\pi^-X$  where the  $X$  system has a low baryonic mass, and the  $\pi^+\pi^-$  pair is misidentified as an  $e^+e^-$  pair.

The case of  $\bar{p}p \rightarrow e^+e^-$  on a free proton at rest has been studied in detail [27] in view of future measurements of the timelike proton form factors in  $\bar{P}$ ANDA. The exclusive process  $\bar{p}p \rightarrow \pi^+\pi^-$  is the dominant background to this measurement, with a cross section  $\sim 10^6$  larger than the  $\bar{p}p \rightarrow e^+e^-$  cross section in the HESR energy range. Simulation studies have been performed in order to estimate precisely the fraction of  $\bar{p}p \rightarrow \pi^+\pi^-$  events that can be eliminated by PID cuts. The most efficient elements for  $\pi^\pm/e^\pm$  discrimination are the electromagnetic calorimeters and the  $dE/dx$  measurements in the tracking systems. Applying the global PID cut at the ‘‘very tight’’ level<sup>2</sup> yields an efficiency to single electrons of  $\sim 90\%$  with a contamination rate of pions smaller than  $10^{-3}$ , for particle momenta above 1 GeV/c [25]. As a result, a rejection factor of  $10^{-7}$  is reached on the pion pair of the process  $\bar{p}p \rightarrow \pi^+\pi^-$ . This background is further reduced by a factor 50-100 when performing a two-body kinematical fit. In this way one obtains a more than 99%

<sup>2</sup> corresponding to a global identification probability greater than 99.8% for an  $e^+$  or an  $e^-$ .

clean sample of  $\bar{p}p \rightarrow e^+e^-$  events, with a 20-30% global efficiency [27].

These results cannot be extrapolated directly to the case of reaction (1), for which a detailed simulation would be required. Nonetheless, the strategy is based on the same elements. In a simplified scheme, the use of the ‘‘very tight’’ PID cut allows to reduce the  $\bar{p}d \rightarrow \pi^+\pi^-n$  hadronic background by a factor  $\sim 10^6$  ( $10^3$  for each charged pion). After that, one is left with a background-to-signal ratio of about 1:1. Kinematical constraints are less efficient than in the case of  $\bar{p}p \rightarrow e^+e^-$  since we have a three-body final state. Here only one constraint can be imposed, on the missing mass. Therefore the remaining background from hadronic processes cannot be eliminated by a cut, it has to be calculated and subtracted. It is in principle possible, provided that the cross section for these processes is measured (in  $\bar{P}$ ANDA) and the PID performances of the detector are known with accuracy. Other reactions due to strong  $\bar{p}n$  annihilation are also potential sources of background. For example the process  $\bar{p}n \rightarrow \pi^-\pi^0$  followed by  $\pi^0$  Dalitz decay, creates a  $\pi^-e^+$  pair that can be misidentified as an  $e^-e^+$  pair; etc.

In summary, the simulations already performed for the channel  $\bar{p}p \rightarrow e^+e^-$  serve as a benchmark study to explore the possibility to measure the process  $\bar{p}d \rightarrow e^+e^-n$  in  $\bar{P}$ ANDA. The competing background to this reaction is certainly more important than in the case of  $\bar{p}p \rightarrow e^+e^-$  on a free proton at rest, and more difficult to reject. We have given elements for a strategy, but the full experimental feasibility remains to be proven. A further study of this point will require complex simulations which are beyond the scope of this paper.

### 3.4 First-order simulation of $\bar{p}d \rightarrow e^+e^-n$

A simple Monte-Carlo simulation of reaction (1), of pure phase-space type, was performed. The detector resolution is implemented in order to estimate some important parameters, such as the achievable resolution in missing mass ( $\sigma_{M_X}$ ) and in dilepton mass ( $\sigma_M$ ).

Kinematics are defined by an incoming antiproton of 1.5 GeV/c momentum onto a deuteron nucleus at rest. The two-body reaction  $\bar{p}d \rightarrow n\gamma^*$  is generated by sampling in  $\cos\theta_{\gamma^*cm}$  (the polar angle) and in the azimuthal angle  $\phi_{\gamma^*cm}$  in the  $\bar{p}d$  center-of-mass. The photon virtuality  $Q^2 = (\mathcal{M})^2$  is sampled between  $Q_{min}^2 = 4m_e^2$  and  $Q_{max}^2 = (\sqrt{s_{\bar{p}p}} - m)^2$ . Then the decay  $\gamma^* \rightarrow e^+e^-$  is generated in the  $\gamma^*$  center-of-mass by sampling in  $\cos\theta_{e^-}$  and  $\phi_{e^-}$ . Finally all the produced particles are transformed back to the laboratory frame. The five samplings are made in uniform distributions, therefore the event weight is not realistic for this first study.

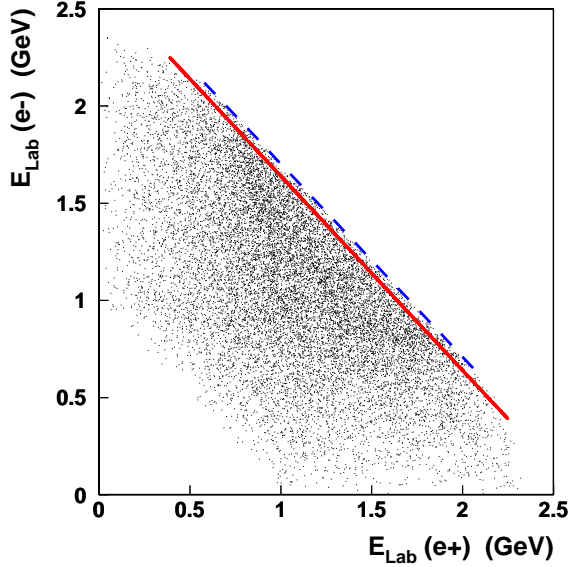


**Figure 8.** Simulation of the reaction  $\bar{p}d \rightarrow e^+e^-n$  at antiproton beam momentum  $p_{\bar{p},lab} = 1.5$  GeV/c: electron energy versus positron energy in the Lab frame. The solid line corresponds to our threshold kinematics of interest (see text). The dashed line corresponds to the reaction  $\bar{p}p \rightarrow e^+e^-$  on a free proton at rest, at the same value of  $p_{\bar{p},lab}$ .

The detector resolution is implemented on the momentum and angles of the electron and positron produced at the vertex, by sampling a measurement error in a Gaussian distribution, independently for  $(p, \theta, \phi)_{Lab}$  of each particle. For the relative momentum resolution  $(\sigma_p/p)$  we take a uniform value of 1.5% in r.m.s., which should be conservative given the rather low momenta involved ( $p \leq 2.2$  GeV/c). The angular resolution is taken to be  $\sigma_\theta = \sigma_\phi = 3mr$  in r.m.s.

The resulting phase space of the lepton pair is shown in fig. 8 for the energies and in fig. 9 for the polar angles. When compared to the case of the reaction  $\bar{p}p \rightarrow e^+e^-$  on a free proton at rest (dashed curves), now most of the correlations between the two leptons are lost and the phase space is much more open. The special threshold kinematics of interest in reaction (1) is defined by: *i*) a photon virtuality corresponding to the  $N\bar{N}$  threshold, i.e.  $\mathcal{M} = 2m$ , and *ii*) the virtual photon emitted at forward angle in the lab (cf. sect. 2.2: this corresponds to  $z = 1$  or  $k = k_{min}$  in the deuteron momentum distribution  $n(k)$ ). For this particular kinematics, represented by a solid curve on Figs. 8 and 9, lepton-to-lepton correlations are re-established, but they differ from the case of a free proton at rest, because the target proton is now off-shell in the deuteron.

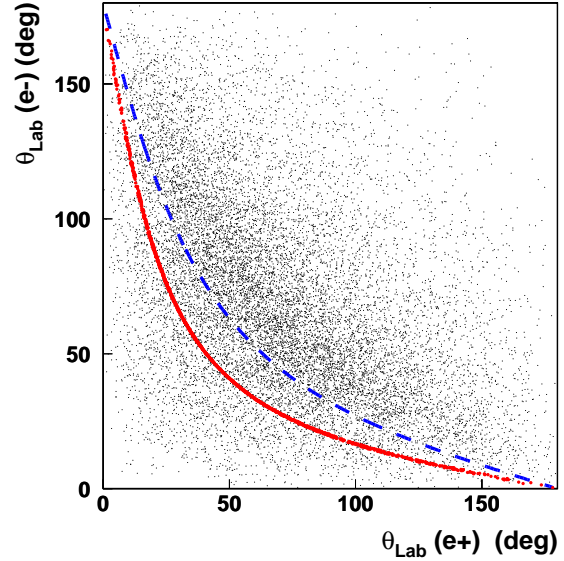


**Figure 9.** Simulation of the reaction  $\bar{p}d \rightarrow e^+e^-n$  at  $p_{\bar{p},lab} = 1.5$  GeV/c: polar angle of the electron versus polar angle of the positron in the Lab frame. The solid curve corresponds to our threshold kinematics of interest (see text). The dashed curve corresponds to the reaction  $\bar{p}p \rightarrow e^+e^-$  on a free proton at rest, at the same value of  $p_{\bar{p},lab}$ .

The off-shellness of the initial proton in process (1) has been defined in sect. 2.2. In the impulse approximation, the off-shell mass squared of this proton is equal to  $t = (p_d - p_n)^2$ , where  $p_d$  and  $p_n$  are the four-momentum vectors of the initial deuteron and final neutron. In this approximation, the proton off-shellness is an experimentally accessible quantity since the neutron is “measured” as the missing particle. Figure 10 shows the  $t$  variable as a function of the photon virtuality, in the full phase space. In the threshold kinematics of interest,  $t$  is equal to  $0.63$  GeV<sup>2</sup> (to be compared with the free proton case,  $t = M_p^2 = 0.88$  GeV<sup>2</sup>).

Finally, fig. 11 shows the experimental resolution that can be expected on the most important variables: the missing mass  $M_X$  and the dilepton invariant mass  $\mathcal{M}$ . These resolutions are quite uniform within the reaction phase space, apart from a slight  $Q^2$ -dependence. The width of the distributions in fig. 11 is dominated by the momentum resolution of the detected  $e^+e^-$  pair. The obtained resolution in missing mass is rather good, with an r.m.s. of 46 MeV, or a full-width at half-maximum of 106 MeV. This value is smaller than one pion mass, therefore by applying a cut around the neutron mass in the  $M_X$  spectrum one should be able to separate - at least partly - the

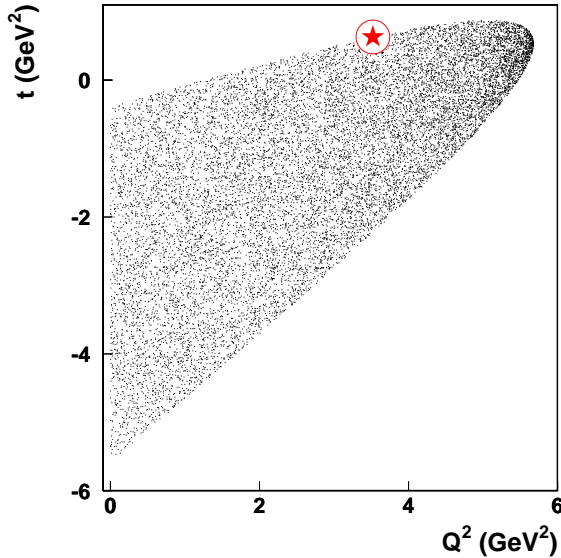


**Figure 10.** Simulation of the reaction  $\bar{p}d \rightarrow e^+e^-n$  at  $p_{\bar{p},lab} = 1.5$  GeV/c: the variable  $t$  (see text) versus the photon virtuality  $Q^2 = (\mathcal{M})^2$ . The circled star corresponds to our threshold kinematics of interest, where  $t = 0.63$  GeV<sup>2</sup>.

missing systems  $X$  of the type (one nucleon + one pion), which are the closest in the spectrum.

The resolution in dilepton invariant mass (r.m.s.= 17 MeV) is also reasonably good, and well suited to evidence some structures due to possible baryonium bound states near the  $p\bar{p}$  threshold.

#### 4 Other aspects

In this paper we have concentrated mostly on the possibility to use process (1) to access the  $p\bar{p}$  threshold and under-threshold region. However, we would like to stress that this process is also interesting for other purposes.

First, it provides a full range of  $e^+e^-$  invariant mass  $\mathcal{M}$  with one single antiproton beam energy. In this sense, the role of the nucleus is a bit similar to the role of initial state radiation in the inverse reaction  $e^+e^- \rightarrow p\bar{p}\gamma_{ISR}$ . As a consequence, any clean experimental data on process (1) at any beam energy (e.g. HESR momenta higher than 1.5 GeV/c), have the potential to yield valuable information on the (half off-shell) nucleon timelike form factors, in a large  $Q^2$ -range. Of course, in this perspective more theoretical work is needed to test the validity of the impulse approximation, and to better define the off-shell effects in the  $N\bar{N}\gamma^*$  vertex.

Second, one should note that the antiproton momentum 1.5 GeV/c just corresponds to the threshold value of

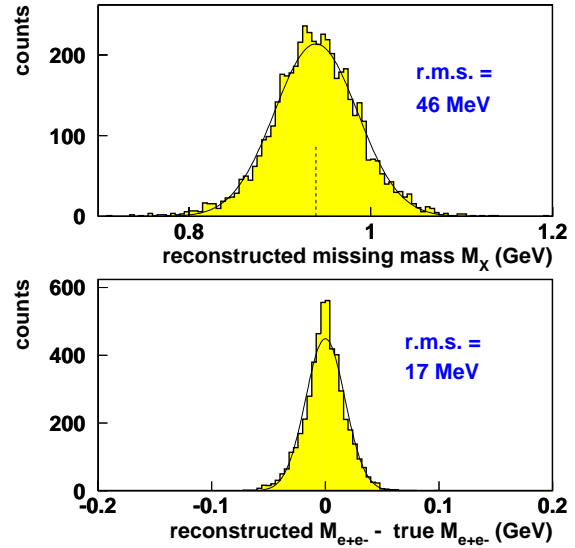


**Figure 11.** Simulation of the reaction  $\bar{p}d \rightarrow e^+e^-n$  at  $p_{\bar{p},lab} = 1.5$  GeV/c: resolution obtained for the missing mass  $M_X$  (upper plot) and for the dilepton invariant mass  $\mathcal{M}$  ( $\equiv M_{e^+e^-}$ , lower plot).

creation of the  $\Lambda\bar{\Lambda}$  pair on a free proton. Therefore the virtual creation of the  $\Lambda\bar{\Lambda}$  pair in reaction (1) is not suppressed by the nucleon momentum distribution in deuteron and contributes just in the domain of the peak of fig. 5, that allows one to study the  $\Lambda\bar{\Lambda}$  threshold region with good statistics. In the  $\Lambda\bar{\Lambda}$  system, the quasi-nuclear states were predicted in [28] and, similarly to the  $N\bar{N}$  quasi-nuclear states, they should manifest themselves as irregularities in the cross section. The contribution of the channel  $\bar{p}p \rightarrow \bar{\Lambda}\Lambda \rightarrow e^+e^-$  in the total cross section  $\bar{p}p \rightarrow e^+e^-$  (the latter equals 1 nb, see sect. 2.2 above) was estimated in [29] as 0.1 nb, i.e. 10% of the total cross section. Therefore we expect that the structures caused by the channel  $\bar{p}p \rightarrow \bar{\Lambda}\Lambda \rightarrow e^+e^-$  can be observed in process (1) in the region of mass  $\mathcal{M}$  near the  $\Lambda\bar{\Lambda}$  threshold.

#### 5 Conclusion

We have studied the reaction  $\bar{p}A \rightarrow (A-1)\gamma^*$  (followed by  $\gamma^* \rightarrow e^+e^-$ ). This process gives access to the  $\bar{p}p$  annihilation  $\bar{p}p \rightarrow \gamma^*$  at invariant masses  $\sqrt{s_{\bar{p}p}}$  which are below the physical threshold of  $2m$ , due to the proton off-shellness in the nucleus. In this way a possibility exists to access the proton timelike form factors in the near-threshold and the totally unexplored under-threshold region, where  $N\bar{N}$  bound states are predicted.

The differential cross section  $d\sigma/d\mathcal{M}$  has been calculated as a function of the dilepton invariant mass  $\mathcal{M}$ , for an incident antiproton of 1.5 GeV/c momentum on a deuteron target (and heavier nuclei). The calculation is done in the impulse approximation; then the distribution of  $\mathcal{M}$  is obtained from the deuteron wave function  $\psi(k)$ . We find that the  $p\bar{p}$  threshold ( $\mathcal{M} = 2m$ ) is reached for a minimal proton momentum  $k_{\min}=360$  MeV/c in the nucleus, and at this point the cross section is about 1 pb/MeV. The calculation does not include the form factor effect, which should come as an extra factor.

Experimental aspects have been investigated in the case of a deuteron target, i.e. for the three-body process  $\bar{p}d \rightarrow e^+e^-n$ . We have taken the conditions of the  $\bar{P}$ ANDA project at FAIR-GSI: an antiproton beam momentum of 1.5 GeV/c and the detection of the lepton pair. The count rate in the near-threshold region of  $\mathcal{M}$  is small but not negligible. The main difficulty is to identify the reaction among the hadronic background which is about six orders of magnitude higher. First elements of strategy were presented for this background rejection, based on particle identification, detector hermeticity, and missing mass resolution. Although the subject would require a much more detailed study, we conclude that this process has a chance to be measurable in  $\bar{P}$ ANDA, given the very good design performances of the detector.

## Acknowledgements

We would like to thank the GDR-Nucléon (n<sup>o</sup> 3034) for providing the infrastructure for this work and financial support. This work is supported in part by the French CNRS/IN2P3.

The authors are indebted to O.D. Dalkarov for his interest to this work, for stimulating discussions and useful advices and to J.-F. Mathiot for his support.

V.A.K. is sincerely grateful for the warm hospitality of the Laboratoire de Physique Corpusculaire, Université Blaise Pascal, Clermont-Ferrand, France, where part of this work was performed. V.A.K. is indebted to A.N. Antonov for illuminating discussions and for kindly providing the data on the nuclear momentum distributions [23,24].

H.F. would like to thank the  $\bar{P}$ ANDA Group at IPN-Orsay, and especially T.Hennino, for useful experimental advices.

## References

1. R. Baldini, et al., Nucleon time-like form factors below the N anti-N threshold, Eur. Phys. J. C11 (1999) 709–715.
2. H. W. Hammer, U.-G. Meissner, D. Drechsel, Dispersion-theoretical analysis of the nucleon electromagnetic form factors: Inclusion of time-like data, Phys. Lett. B385 (1996) 343–347.
3. C. Adamuscin, S. Dubnicka, A. Z. Dubnickova, P. Weisenpacher, Unitary and analytic model of nucleon EM structure, the puzzle with JLab proton polarization data and new insight into proton charge distribution, Prog. Part. Nucl. Phys. 55 (2005) 228–241.
4. F. Iachello, Q. Wan, Structure of the nucleon from electromagnetic timelike form factors, Phys. Rev. C69 (2004) 055204.
5. R. Bijker, F. Iachello, Re-analysis of the nucleon space- and time-like electromagnetic form factors in a two-component model, Phys. Rev. C69 (2004) 068201.
6. U.-G. Meissner, Baryon form-factors: Model independent results, Nucl. Phys. A666 (2000) 51–60.
7. O. D. Dalkarov, K. V. Protasov,  $e^+e^-$  annihilation near  $\bar{N}N$  threshold, Nucl. Phys. A504 (1989) 845–854.
8. O. D. Dalkarov, K. V. Protasov, On the new vector state in  $e^+e^-$  annihilation near 2-GeV, Mod. Phys. Lett. A4 (1989) 1203.
9. I. S. Shapiro, The Physics of Nucleon - anti-Nucleon Systems, Phys. Rept. 35 (1978) 129–185.
10. G. Bardin, et al., Determination of the electric and magnetic form-factors of the proton in the timelike region, Nucl. Phys. B411 (1994) 3–32.
11. B. Aubert, et al., A study of  $e^+e^- \rightarrow p$  anti- $p$  using initial state radiation with BABAR, Phys. Rev. D73 (2006) 012005.
12. O. D. Dalkarov, V. G. Ksenzov, A possibility of deriving the electromagnetic proton form-factor in the nonphysical region from reactions with deuteron (in Russian), Pisma Zh. Eksp. Teor. Fiz. 31 (1980) 425–429, JETP Lett. Vol.31 Num. 7 (1980) 397–400.
13. M. Schafer, H. C. Donges, U. Mosel, Electromagnetic form-factor of the nucleon in the timelike region, Phys. Lett. B342 (1995) 13–18.
14. C. Adamuscin, E. A. Kuraev, E. Tomasi-Gustafsson, F. E. Maas, Testing axial and electromagnetic nucleon form factors in time-like regions in the processes  $\text{anti-}p + n \rightarrow \pi^- + l^- + l^+$  and  $\text{anti-}p + p \rightarrow \pi^0 + l^- + l^+$ ,  $l = e, \mu$ , Phys. Rev. C75 (2007) 045205.
15. A. Z. Dubnickova, S. Dubnicka, M. P. Rekalov, Investigation of nucleon electromagnetic form-factors in the unphysical region by means of the  $\text{anti-}N N \rightarrow \pi$  lepton+ lepton- reactions, Z. Phys. C70 (1996) 473–482.
16. H. W. L. Naus, J. H. Koch, Electromagnetic interaction of an off-shell nucleon, Phys. Rev. C36 (1987) 2459–2465.
17. P. C. Tiemeijer, J. A. Tjon, Electromagnetic form-factors for an off-shell nucleon in a vector meson dominance model, Phys. Rev. C42 (1990) 599–609.
18. O. D. Dalkarov, V. A. Karmanov, 2008 (unpublished).
19. J. Carbonell, B. Desplanques, V. A. Karmanov, J.-F. Mathiot, Explicitly covariant light-front dynamics and relativistic few-body systems, Phys. Rept. 300 (1998) 215–347.
20. J. Carbonell, V. A. Karmanov, Relativistic deuteron wave function in the light front dynamics, Nucl. Phys. A581 (1995) 625–653.

21. R. Baldini, S. Pacetti, A. Zallo, A. Zichichi, Unexpected features of  $e^+e^- \rightarrow p\bar{p}$  and  $e^+e^- \rightarrow \Lambda \bar{\Lambda}$  cross sections near threshold, *Eur. Phys. J. A* 39 (2009) 315–321.
22. R. Baldini, S. Pacetti, A. Zallo, Point-like Baryons? arXiv:0812.3283 [hep-ph].
23. A. N. Antonov, et al., Superscaling, scaling functions and nucleon momentum distributions in nuclei, *Phys. Rev. C* 71 (2005) 014317.
24. A. N. Antonov, et al., Superscaling analysis of inclusive electron scattering and its extension to charge-changing neutrino nucleus cross sections beyond the relativistic Fermi gas approach, *Phys. Rev. C* 74 (2006) 054603.
25. The PANDA Collaboration, Physics Performance Report for PANDA: Strong Interaction Studies with Antiprotons arXiv:0903.3905 [hep-ex].
26. The PANDA Collaboration, Technical Progress Report for PANDA, [http://www-panda.gsi.de/archive/public/panda\\_tpr.pdf](http://www-panda.gsi.de/archive/public/panda_tpr.pdf) (2005).
27. M. Sudol, et al., Feasibility studies of the time-like proton electromagnetic form factor measurements with PANDA at FAIR (submitted to EPJA). ArXiv:0907.4478 [nucl-ex].
28. J. Carbonell, K. V. Protasov, O. D. Dalkarov, On a possible near threshold  $\Lambda \bar{\Lambda}$  state, *Phys. Lett. B* 306 (1993) 407–410.
29. O. D. Dalkarov, private communication.